ResearchGate

See discussions, stats, and author profiles for this publication at: https://www.researchgate.net/publication/256191365

Dynamics of Water Confined in Reversed Micelles: Multidimensional Vibrational Spectroscopy Study

ARTICLE *in* THE JOURNAL OF PHYSICAL CHEMISTRY B · AUGUST 2013

Impact Factor: 3.3 · DOI: 10.1021/jp405853j · Source: PubMed

CITATIONS
21

READS
61

6 AUTHORS, INCLUDING:

Artem Bakulin
University of Cambridge
50 PUBLICATIONS **1,276** CITATIONS

SEE PROFILE

Thomas La Cour Jansen
University of Groningen
78 PUBLICATIONS **1,716** CITATIONS

SEE PROFILE

Available from: Thomas La Cour Jansen
Retrieved on: 26 January 2016

THE JOURNAL OF PHYSICAL CHEMISTRY B

Article

pubs.acs.org/JPCB

Dynamics of Water Confined in Reversed Micelles: Multidimensional Vibrational Spectroscopy Study

Artem A. Bakulin,[†] Dan Cringus,[†] Piotr A. Pieniazek,[‡,§] James L. Skinner,[‡] Thomas L. C. Jansen,[†] and Maxim S. Pshenichnikov*[,†]

[†]Zernike Institute for Advanced Materials, University of Groningen, Nijenborgh 4, 9747 AG Groningen, The Netherlands

[‡]Theoretical Chemistry Institute and Department of Chemistry, University of Wisconsin, Madison, Wisconsin 53706, United States

ABSTRACT: Here we perform a comprehensive study of ultrafast molecular and vibrational dynamics of water confined in small reversed micelles (RMs). The molecular picture is elucidated with two-dimensional infrared (2D IR) spectroscopy of water OH stretch vibrations and molecular dynamics simulations, bridged by theoretical calculations of linear and 2D IR vibrational spectra. To investigate the effects of intermolecular coupling, experiments and modeling are performed for isotopically diluted (HDO in D_2O) and undiluted (H_2O) water. We put a separation of water inside RMs into two subensembles (water-bound and surfactant-bound molecules), observed by many before, on a solid theoretical basis. Water molecules fully attached to the lipid interface ("shell" water) are decoupled from one another and from the central water nanopool ("core" water). The environmental fluctuations are largely "frozen" for the shell water, while the core waters demonstrate much faster dynamics but still not as fast as in the bulk case. A substantial nanoconfinement effect on the dynamics of the core water is observed after disentanglement of the shell water contribution, which is fully confirmed by the simulations of 2D IR spectra. Current results provide new insights into interaction between biological objects like membranes or proteins with the surrounding aqueous bath, and highlight peculiarities in vibrational energy redistribution near the lipid surface.

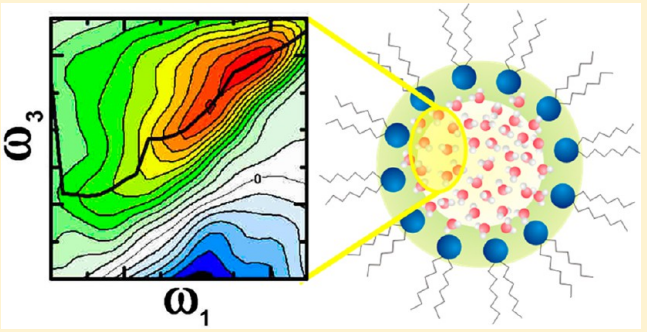

INTRODUCTION

Hydration shells of biological membranes are important for the wide range of chemical and biochemical processes including surface-specific reactions, protein secondary structure stabilization, and proton and energy transfer. The membrane−water interface is usually pictured as a layer of lipids bordering a homogeneous bath of water molecules strongly coupled by the hydrogen bonds.[1] In the last decades, a number of studies challenged this concept.[2,3] Various experiments have indicated[4,5] that a broad distribution of water sites exists inside the lipid layer, thereby forming a constitutive part of a membrane. It has also been shown that water mobility and hydrogen-bond dynamics near the lipid interface are substantially different from the bulk water.[6−8]

An example and at the same time a model system for water confined by a lipid interface is presented by reverse micelles (RMs)—nanometer scale droplets of water separated from the surrounding nonpolar environment by a monolayer of amphiphilic lipid molecules.[9] RMs are currently extensively used and studied in different areas of chemical, biological, and material sciences due to the confinement effect RMs provide on the internal aqueous environment.[10,11] The easiness of RM size manipulation provides a flexible tool to control the extent of water confinement, by simply changing the ratio w between amounts of water and surfactant in the micelle emulsion. In small ($w = 2$; diameter of $d = 1−2$ nm) RMs, most of the water molecules are located in the first or second solvation shells of the water−lipid interface,[12,13] which makes such RMs a model system for spectroscopic studies of so-called "biological" water, e.g., water in the confined and crowded environment of living cells with the hydrogen-bond network affected by various solutes, lipid membrane interfaces, and high concentration of counterions. In contrast, water properties in large ($d > 10$ nm, $w \geq 30$) RMs approach those of the bulk state, which, in particular, makes large RMs useful for studying bulk water dynamics[14] without need for nanocells[15] to handle sample optical density.

The specificity of the water environment of RMs is determined by the geometry and by the dynamics[16] of the water hydrogen-bond network which is known to occur on the broad variety of the time scales ranging between 0.1 and 100 ps.[16−21] For this reason, ultrafast dynamics of water in RMs has attracted a lot of attention, both from spectroscopic and theoretical points of view.[22] Experimental studies have been aimed at directly resolving changes in water environment on the ultrafast time scale, usually by tracing in time vibrational

Special Issue: Michael D. Fayer Festschrift

Received: June 13, 2013
Revised: August 27, 2013

ACS Publications © XXXX American Chemical Society

dx.doi.org/10.1021/jp405853j | J. Phys. Chem. B XXXX, XXX, XXX−XXX

dynamics of water molecules.[17,21,23−35] Theoretical studies, until now, have mostly been focused on applying molecular dynamics (MD) models to elucidate molecular level motions of water in the RMs.[12,36−40] As a validity criterion for these models, time-averaged macroscopic parameters produced by the simulations were confronted to those deduced from the NMR,[41] neutron scattering,[42] or linear infrared absorption experiments.[43]

Most previous experimental and theoretical studies indicated that the nanodroplet interior of RMs consists of the "bulk-like" water in the micelle core and a fraction of "shell" water near the lipid interface, where water molecules are less bound with each other and more to the lipid interface. The separation of water on two subensembles was first observed in NMR experiments and molecular dynamics (MD) simulations performed on the RMs.[12,44] Ultrafast spectroscopy of water vibrations in RMs exposed a noticeable slowing down of vibrational relaxation rates and rotational dynamics of water with decreasing size of RMs.[30,32,34,45,46] It was proposed that this evidences a nanoconfinement effect due to reduction of the amount of interacting water molecules to a finite number (typically, several tens).[31] Another explanation of slowing down dynamics with decreasing RM size is the increased contribution from the interfacial shell water which is considerably slower than the bulk one.[33,45] Therefore, nanoconfined core water can be claimed only after disentangling the contributions from the "slow" shell and "fast" core waters. This gives rise to the following dilemma: in large RMs, the influence of the shell water is rather limited, but the nanoconfinement effect is small because of many water molecules in the core, while, in small RMs, the nanoconfinement is expected to be large, but it is screened by the relatively strong and slow contribution from the shell water.

Detailed information about the dynamics of the hydrogen bond network in an aqueous environment of RMs can also be derived by using the frequency of water stretches as a reporter for the strength of hydrogen bonds in which a water molecule is involved.[47] Measurements of the hydrogen bond dynamics are to be performed on sub-ps time scale characteristic and also require a contrast parameter for differentiating subensembles of waters with different hydrogen-bond configurations (and therefore possessing different vibrational frequencies) to trace their time evolution. Coherent 2D IR spectroscopy directly addresses these issues by producing information about the correlations in the vibrational response of the water in different moments of time.[15,48−50] In a 2D IR experiment, first, a pair of pump pulses separated by a well-controlled "coherence" time t_{12} is created in a sample vibrational population; the population spectrum (frequency grating) in ω_1 excitation-frequency space is determined by the coherence time. After the waiting time T, the changes in the frequency grating, induced by system dynamics, are probed by another pair of pulses. The generated signal is detected via a spectrally resolved interferometry (optical heterodyning) providing the probe frequency axis ω_3. The excitation (pump) frequency axis ω_1 is calculated through Fourier transformation of the coherence time t_{12}. The resulting 2D map correlates the initial frequencies of vibrationally excited oscillators with the respective frequencies after the waiting time T. Maintaining high time resolution, 2D IR spectroscopy also retains high spectral resolution, which allows separating signals of different origin, such as ground and excited state transitions, effects of sample heating, anharmonic couplings, etc.

First 2D IR experiments on RMs were recently reported by us[51] and Fayer and co-workers indicating slow vibrational frequency dynamics of the micelle-confined water[52] and surrounding membrane.[20,53] The recorded 2D IR spectra contain impressive amounts of information about the dynamics of vibrational excited states. However, the interpretation of this information is intricate, because 2D IR observables originate from entangled contributions of different origins. These contributions include changes in the bond strength due to molecular motions of water, non-Condon effects, inter- and intermolecular couplings between different vibrational oscillators, coupling to librational degrees of freedom, and even delocalization of vibrational excitations.[43,47] This highlights the importance of linking the outcome of 2D IR experiments to the molecular picture of water through the accurate modeling of water vibrational dynamics and spectroscopic observables. Such an approach is especially important for the studies where pure water rather than an isotopic mixture is utilized. In pure water, intermolecular coupling between vibrational modes of different water molecules allows vibrational excitation to delocalize from the initially excited oscillator, which complicates the interpretation of the observed dynamics.[15,54] On the other hand, intermolecular transfer of vibrational energy can be used to elucidate the level of separation between water molecules and the dynamics of the hydrogen bond environment.[55]

RMs have been extensively studied using molecular dynamics (MD) simulations to understand the behavior of nanoconfined water.[40,42,56−60] For the type of RMs studied here, the structures of the formed micelles were typically found to deviate considerably from a spherical shape[40] and the interfacial water was found to associate strongly with the lipid head groups.[59] It is further observed that the counterions are located in the vicinity of the lipid head groups.[56,57,60] The dynamics of the RM interior water are observed to be gradually slowing down as the water molecules approach the lipid interface.[56] A more recent study suggested that the computed structure and dynamics is very sensitive to the employed force field.[40] While generally the structure and water dynamics have been investigated, only a single publication has explicitly considered the vibrational IR spectroscopy of these systems.[56] In this study, the linear absorption and anisotropy decay of the OH stretch vibration in isotopically diluted water were simulated with no extension to undiluted water nor to 2D spectroscopy that is more sensitive to dynamics and details of interactions.

Explicitly simulating the vibrational spectra, both 1D and 2D, is crucial for the interpretation of the experimental data as non-Condon effects modulate the absorption strength across the spectra,[61] non-Gaussian effects influence the line shapes,[21] and the vibrational excitations extend over numerous OH stretches leading to excitonic effects that modify both spectral shapes and intensities.[43] Therefore, simplified models that do not explicitly project MD simulations onto spectroscopic observables are insufficient to adequately describe RM spectroscopy and may even lead to unreliable interpretations.

In this paper, we make the next step in further investigation of RM-confined water by measuring, modeling, and interpreting the vibrational frequency dynamics for different subensembles of water molecules, accessed with 2D IR spectroscopy.[62] Spectroscopic experiments were performed on small (w = 2) RMs containing pure as well as isotopically diluted water. At the same time, combined MD-quantum mechanical modeling of RMs of a similar size was performed to evaluate the vibrational dynamics. The calculated 2D IR spectra were

dx.doi.org/10.1021/jp405853j | J. Phys. Chem. B XXXX, XXX, XXX−XXX

compared to the outcome of the 2D IR experiments to verify the correctness of the model used and to disentangle different contributions to experimental observables. In agreement with previous studies, we show that there are two different subensembles (water-bound and lipid-bound) of water molecules with noticeably different dynamics. We show that, in contrast to the bulk water, vibrational transitions of water in RMs display extremely slow dynamics extending to several ps. At this time scale, we do not observe any OH-bond environment change nor intermolecular energy transport within the interfacial water layer. While the lipid-bound waters are isolated from the aqueous reservoir, water molecules in the core of the micelles still form a hydrogen-bonded network but experience a strong nanoconfinement effect.

EXPERIMENTAL METHODS

To probe the dynamics of the hydrogen bond network, we performed 2D IR correlation spectroscopy experiments on the environment-sensitive OH stretch vibrations of H_2O and HDO molecules. In our experiments, infrared pulses were produced by an optical parametrical generator[63] pumped by a 1 kHz Ti:sapphire multipass amplifier. The mid-IR pulses were tunable around 3500 cm^{-1} and had a duration of about 70 fs with a bandwidth of ~350 cm^{-1} (fwhm) which is enough for a virtually impulsive excitation/probe. The generated pulses were split in three 3 μJ pulses and one <0.1 μJ local oscillator pulse. Then, after passing the interferometer-controlled delay stages, all the pulses were focused into the 50 μm wire-guided jet[64] sample. During the experiment, for each value of the evolution time T, coherence time τ_1 was scanned in ±0.6 ps range with 1 fs steps, and the interference between the four-wave mixing signal and the local oscillator was recorded by a 64-element MCT array. For accurate distinction between the real and imaginary components in the response, a phasing procedure was applied.[65] First, zero delay $\tau_1 = 0$ in the first pair of pulses was determined with ±2 fs accuracy by measuring IR photon echoes for signals in two phase-matching directions;[66] then, the relative phase shift and the real part of the response were identified by matching the $\delta\omega_1$ integral of the 2D IR spectrum to the independently measure broadband-pump−probe spectrum. All experiments were performed at ambient conditions.

RMs were prepared by mixing appropriate amounts of HPLC grade water, bis(2-ethylhexyl) sulfosuccinate (AOT) obtained from Aldrich, and octane (Janssen Chimica). For RMs with isotopically diluted water, 5% solution of HDO in D_2O was used instead of H_2O. All substances were used as received, without any further purification. For all samples, the water concentration was about 0.3 mol/L, which corresponds to a maximal optical density of about 0.4 at the measurement frequency.

Numerical Simulations. For numerical simulations, we used the $w = 2$ RM molecular dynamics trajectory obtained in a previous study.[56] In these simulations, 52 water molecules were surrounded by 26 AOT molecules, 26 sodium counterions, and 357 iso-octane molecules. The water molecules were described with the SPC/E force field.[67] The sodium parameters were taken from Schweighofer.[68] The AOT alkyl chains and iso-octane were described with the TraPPe force field.[69,70] The sulfonate headgroups were modeled with the CHARMM force field.[71] Time steps of 1 fs were used during the simulation. The temperature was fixed at 300 K and the pressure at 1 atm using the Berendsen method.[72] Electrostatic interactions were treated using particle-mesh Ewald summation. Lennard-Jones interactions were smoothly switched to 0 between 1.5 and 1.9 nm. All other simulation details are given in ref 56. A snapshot from the simulation is shown in Figure 1.

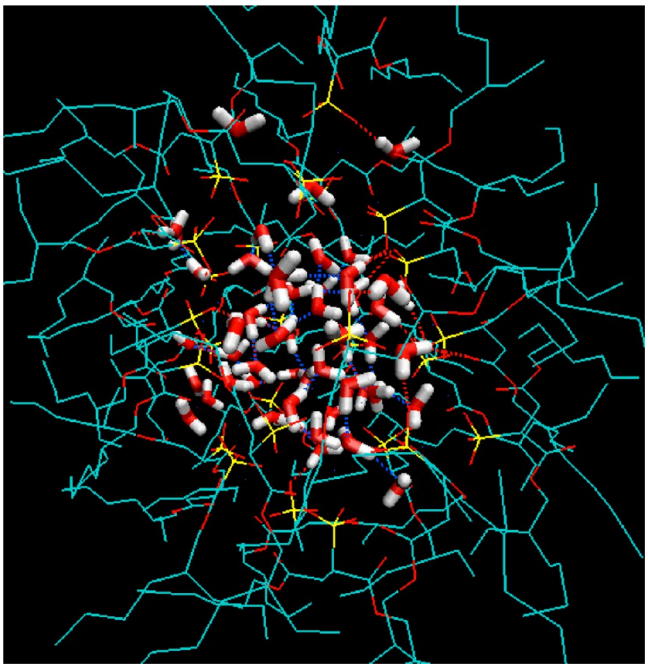

Figure 1. Schematics of the interior of the simulated RM. The 52 water molecules are highlighted in bold. The 26 AOT molecules are represented with thin lines. The 357 iso-octane molecules are not shown. The drawings were made with the VMD program[107] using the standard color settings: oxygen is red, hydrogen is white, sulfur is yellow, and carbon is cyan. Hydrogen bonds donated by water to another water molecule or sulfonate group are shown with dashed lines in blue and red, respectively.

For the spectral simulations, the OH stretches are treated with floating oscillator modes using the time-dependent Hamiltonian:

$$H = \sum_i^N \omega_i(t) B_i^+ B_i + \sum_{i,j}^N J_{ij}(t) B_i^+ B_j - \sum_i^N \frac{\Delta_i(t)}{2} B_i^+ B_i^+ B_i B_i + \sum_i^N \vec{\mu}_i(t)\cdot\vec{E}(t)(B_i^+ + B_i) + \vec{\mu}_i^{12}(t)\cdot \vec{E}(t)(B_i B_i^+ B_i^+ + B_i^+ B_i B_i) \quad (1)$$

Here, B_i^+ and B_i are bosonic creation and annihilation operators. The fundamental frequency ω_i for each OH stretch is determined from an electronic structure-based electrostatic map relating it to the electric field generated by the surrounding molecules along the OH bond.[56] In reality, an effective electric field was used, where the effects from cations and anions were scaled slightly.[56] The effective electric field is

$$E_{\text{eff}} = E_{H_2O} + 0.81379E_+ + 0.92107E_- \quad (2)$$

where E_{H_2O} , E_+, and E_- are the electric fields generated by water, cations, and anions, respectively. When i and j denote OH stretches within the same molecule, J_{ij} is the intramolecular coupling, which is determined by an electrostatic map depending on the electric fields along both OH bonds.[73] If i and j are OH stretches on different water molecules, J_{ij} is the

dx.doi.org/10.1021/jp405853j | J. Phys. Chem. B XXXX, XXX, XXX−XXX

intermolecular coupling determined by the transition dipole interaction.[73] The anharmonicity Δ_i and the transition dipoles μ and μ^{12} are determined by an electrostatic map depending on the electric field along the OH bond.[74] The transition dipole term μ^{12} accounts for the deviation of the overtone transition dipole from the harmonic rule.[43,56] From the full 10 ns MD trajectory, 10 subtrajectories were extracted with 1 ns between them. Each 50 ps subtrajectory contained the time-dependent Hamiltonian saved at 10 fs time intervals.

The linear absorption and two-dimensional infrared spectra were obtained with the numerical integration of the Schrödinger equation method (NISE).[75,76] This was done with a new sparse matrix implementation designed for application to large systems.[43] In brief, the third-order time-domain response functions governing the two-dimensional infrared spectra are calculated by solving the time-dependent Schrödinger equation numerically by dividing the time into short intervals during which the Hamiltonian can be treated as a constant. Then, the time-dependent Schrödinger equation is solved for each time interval with the time-independent Hamiltonian. By combining the results for each short time interval, the time evolutions for longer times are obtained and the response functions calculated. These time-domain response functions are then Fourier transformed to give the two-dimensional infrared spectra. The calculations were accelerated using the sparse matrix scheme described in ref 43. The same truncation parameter for the elements of the time-evolution matrix as in that study was used neglecting values with a magnitude below 1.2×10^{-5}. For each subtrajectory, the 2D IR spectra were sampled 97 times providing a total of 970 samples for each spectrum. The coherence times τ_1 and τ_3 were varied from 0 to 400 fs. Orientational averaging over all 21 molecular frame laser polarization arrangements[77] was performed.

Linear IR Spectra. Figure 2 shows experimental and calculated absorption spectra in the OH stretching mode region for the w = 2 RM filled either with isotopically diluted water HDO:D_2O (a) or with H_2O (b,c). There are three main differences of these spectra with their bulk water counterparts (not shown). First, both experimental spectra are considerably narrower; second, they are blue-shifted,[43,47] and third, the H_2O-filled RM absorption is broader than the HDO-filled one. All three features are excellently reproduced by simulations. The HDO:D_2O case (Figure 2a), where there are no inter- nor intramolecular couplings between OH oscillators, serves as a benchmark for testing the validity of calculations. In this case, our ability to describe the experimental data with no adjustable parameters (apart from the scaling of the electric field generated by the ions) gives credit to the employed molecular dynamics force fields, and electrostatic frequency and transition dipole maps.

In the H_2O case (Figure 2b,c), the calculations also produce a reasonable result. This case is indeed more difficult to simulate due to intra- and intermolecular couplings between OH vibrations. In particular, the broadening of the spectrum in the high-frequency part can be ascribed to intramolecular coupling of the OH oscillators that belong to the same water molecule. On the other hand, the prominent red shoulder is due to intermolecular coupling of waters, similar to bulk water. To verify this hypothesis, we calculated the absorption spectrum of H_2O in the w = 2 RM with the intermolecular coupling set to zero (Figure 2c) and found that the bandwidth and the red shoulder of the spectrum shrink down. Interestingly, the red flank calculated with no intermolecular

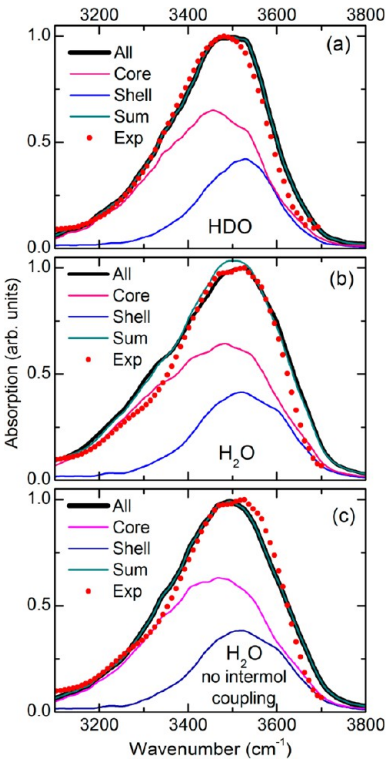

Figure 2. Absorption spectra of the HDO- (a) and H_2O-filled (b, c) w = 2 RMs in the OH stretch region. Red dots show the experimental spectra, while the calculated spectra are depicted as follows: black curves, all contributions are included; magenta curves, the core waters only; blue curves, the shell waters only; dark cyan curves, the sum of the latter two contributions. In part c, the intermolecular coupling between OH stretches was set to zero.

couplings now matches the experimental data much better. This observation signifies that water molecules are probably less coupled to each other than predicted by theory, which can be rationalized by examining the data for which the transition dipole model was parametrized in ref 78. It is likely that the transition dipole approximation overestimates the coupling when water molecules are very close which is a known drawback of the applied model.

For further discussion, it is instructive to divide 52 considered water molecules into subensembles. We have tested several different options (for instance, the subensembles were defined as to what particular molecule the hydrogen bond is donated or to the number of hydrogen bond of the molecule), and finally opted for the following two subensembles. The first one contains all water molecules that donate at least one hydrogen bond to another water molecule (Figure 3a,b). Such water molecules are expected to be in or near the center of the RM. The second subensemble contains all other water molecules including water molecules without hydrogen bonds, water molecules donating hydrogen bond(s) to the AOT sulfonate groups, and water molecules donating hydrogen bond(s) to the AOT carbonyl groups (Figure 3c,d). These subdivisions echo the conventional "core−shell" model, the validity of which has been proven in many studies,[30,32,45,79] but now with the two subensembles being rigorously defined. A number of hydrogen bonding criteria have been proposed; here, we use one based on charge transfer to the σOD(H)* orbital of the hydrogen bond donor molecule.[74,80] Note, nonetheless, that the current definition that uses a HB criterion

dx.doi.org/10.1021/jp405853j | J. Phys. Chem. B XXXX, XXX, XXX−XXX

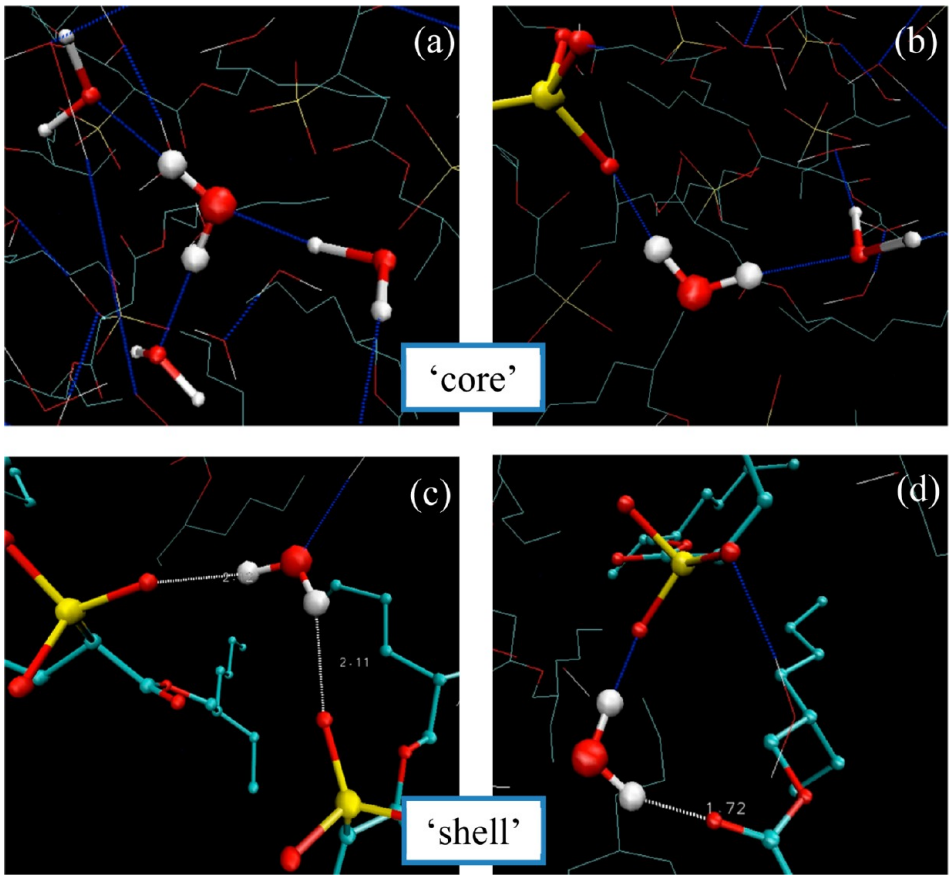

Figure 3. Partitioning of waters into the core (a, b) and shell (c, d) subensembles. The core waters are defined as those donating two (a) or one (b) hydrogen bond to another water molecule. The shell waters are those which do not donate any single hydrogen bond to another water but to oxygens of the sulfunate groups (c) or of the carbonyl groups (d) or donate no hydrogen bond at all (not shown). The color codes are the same as in Figure 1

is at variance with the previous nomenclature[74] that uses the geometric criterion. For instance, for a $w = 2$ RM, the latter criterion results in ~0.2 fraction of the core (i.e., bulk-like) molecules, while the current criterion yields the ~0.6 fraction of the core molecules.[81]

The main motivation of the proposed subdivision is the fact that the core and the shell do not interact with each other in a spectroscopic sense. This means that, if the core and shell subensemble contributions to the absorption spectra are disentangled, their sum results in an absorption profile similar to that calculated for the whole system (Figure 2). In the HDO:D_2O case, this of course holds precisely as the HDO molecules do not interact among themselves (Figure 2a). In the H_2O case, when both the inter- and intramolecular interactions are strong, the sum of core and shell contributions is still virtually identical to the overall absorption (Figure 2b), which proves that there is little interaction between the core and the shell. The sum is slightly narrower due to the intermolecular coupling which is otherwise responsible for broadening of the spectra.

For both HDO:D_2O- and H_2O-filled micelles, the vibrational frequency shift between the core and shell waters is ~75 cm^{-1} (Figure 2). This signifies that the core waters on average have stronger hydrogen bonds. Calculations of the absorption profile with the intermolecular interaction switched off (Figure 2c) allow us to estimate the contribution of the intramolecular interactions. For shell waters, the fwhm width of the absorption contour is ~200 cm^{-1} for HDO:D_2O, ~240 cm^{-1} for H_2O, and ~240 cm^{-1} for H_2O with no intermolecular interactions. Therefore, for the shell, the intermolecular interactions are not as important as the intramolecular ones. In contrast, for the core water, the respective widths are 280, 350, and 310 cm^{-1}, indicating that contributions from inter- and intramolecular couplings are comparable. The suppressed interaction between different subensembles in shell water is in agreement with the previous reports on identification of different water-membrane structural motifs by using 2D IR spectroscopy.[82]

The probability densities of frequency distributions for the two subensembles (core and shell water) are shown in Figure 4. The distributions are characterized by maxima at 3515 and 3575, with the fwhm of the main peak being ~300 and 225 cm^{-1} for the core and shell water, respectively. This shows that the typical frequencies of the shell water molecules are higher than the core water frequencies and at the same time environmental fluctuations are smaller. Furthermore, for the shell water, a high frequency peak at 3770 cm^{-1} with fwhm of only 10 cm^{-1} is observed that represents a small population of water molecules not involved in hydrogen bonding. When comparing with the calculated linear HOD:D_2O spectra of the subensembles also provided in Figure 4, the spectra appear red-shifted by ~50−75 cm^{-1}. This shift arises from the significant non-Condon effects observed in the OH stretch of water.[61] Furthermore, the high-frequency peak at 3770 cm^{-1}, associated with the water molecules not participating in hydrogen bonding, is completely absent in the calculated linear absorption spectrum, again because of the pronounced non-

dx.doi.org/10.1021/jp405853j | J. Phys. Chem. B XXXX, XXX, XXX−XXX

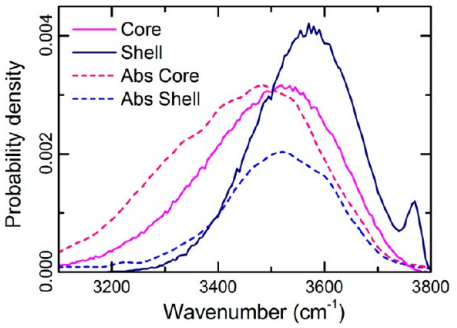

Figure 4. The local OH frequency distributions (solid) and the simulated linear absorption HOD spectra (dashed) for the core (blue) and shell (pink) water subensembles. Note that the absorption spectra are red-shifted because of substantial non-Condon effects.

Condon effects. This makes IR absorption spectroscopy not particularly sensitive to the small population of such species.

2D IR Spectra. Figures 5 and 6 (upper panels) show experimental absorptive 2D IR spectra of H_2O- and HDO:D_2O-filled micelles at different evolution times T. The positive signals on the diagonal (coded in green-yellow-red) represent bleaching of the 0−1 transition from ground state and stimulated emission from the first excited state. The excited state absorption is depicted as a negative signal (coded in blue-black) shifted along the ω axis by the anharmonicity value of ~200 cm^{-1}. At longer (>1 ps) waiting times, the excited state absorption peak becomes less prominent because of the overlap with the additional bleaching, induced by the heating of the sample.

The mechanism of the heating response was identified as the following:[32] upon vibrational relaxation of the OH stretch, the energy is rapidly (within 1 ps) redistributed among low-frequency (collective) modes, which is equivalent to the temperature increase of the reversed micelle.[32] Because the OH stretch absorption is very sensitive to temperature, in a differential measurement, an additional positive peak appears centered at the frequency of $\omega \sim 3450$ cm^{-1}. Fortunately, in small RMs, heating has a local effect[32] and the heat is efficiently transferred away from the water pool through the lipid membrane,[83] thereby limiting the magnitude of the heating response. The heating effect is less prominent in the HDO:D_2O RMs (compare the upper panels in Figures 4 and 5 at $T > 1$ ps) because there are on average only ~2.5 OH oscillators per RM. Therefore, the thermal response is frequency-shifted to the region of the OD stretch absorption (i.e., around 2400 cm^{-1}), while at 3500 cm^{-1} it contributes mostly to the refractive index changes[84] to which the absorption 2D IR is not sensitive. In contrast, in the case of the H_2O-filled RMs, all H_2O molecules contribute to the thermal response, which makes it more significant.

The elongated shapes of the diagonal transition peaks indicate strong inhomogeneous broadening of the OH vibrational transition. Generally, after some evolution time, the elongation decreases as the result of spectral diffusion and finally acquires a completely round shape, associated with an entire loss of phase memory and homogeneous distribution of states. For instance, for bulk water, the dephasing time was established as short as 100 fs,[15] and for HDO:D_2O, the longest correlation time is in the order of 1 ps.[85,86] In contrast, in $w = 2$ RM correlation spectra, the 0−1 transition peak retains an elliptical shape for much longer waiting times. The characteristically inhomogeneous peak shapes can also be partly observed up to 5 ps at the blue side of the spectrum for both H_2O- and HDO:D_2O-filled RMs. This implies that on this time

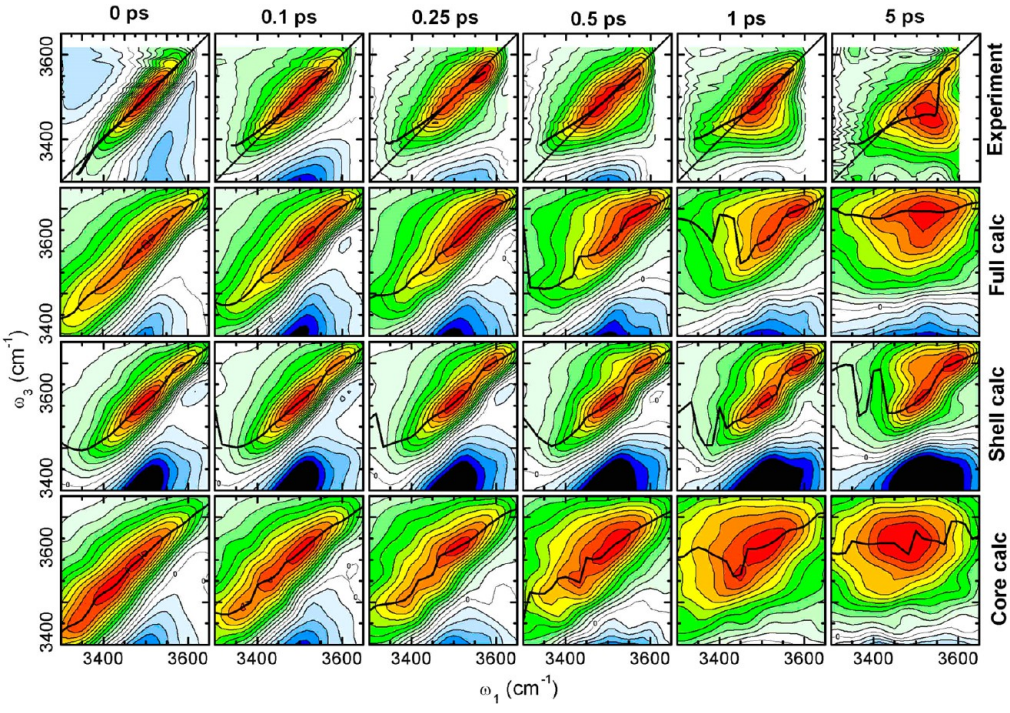

Figure 5. Normalized experimental (upper row) and calculated (lower three rows) absorptive components of 2D IR spectra of H_2O confined in $w = 2$ reversed micelles at waiting times 0, 0.1, 0.25, 0.5, 1, and 5 ps. The second, third, and fourth rows depict results of full calculations, calculations for the shell waters, and calculations for the core waters, respectively. The equilateral contours are drawn with the 8% step of the maximal amplitude. The solid black curves are drawn at maxima of each ω_1-cut.

dx.doi.org/10.1021/jp405853j | J. Phys. Chem. B XXXX, XXX, XXX−XXX

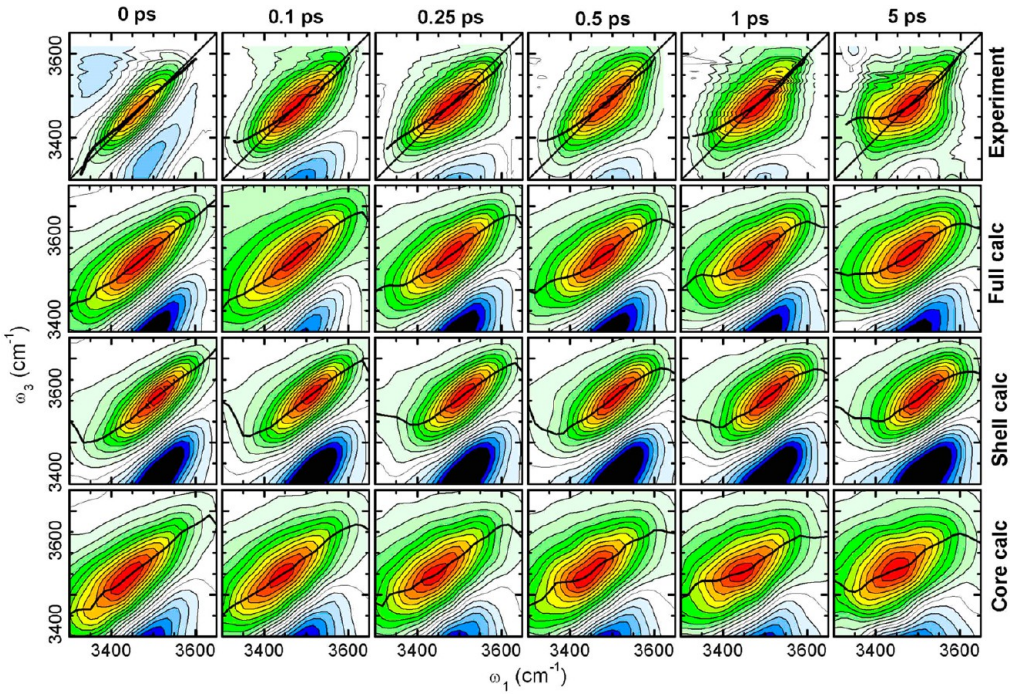

Figure 6. The same as Figure 4 but for the HDO:D_2O-filled reversed micelles.

scale there is no dynamical process which sweeps the OH vibrational frequencies either by washing out the structural variations in the hydrogen bond network or by an energy transfer between H_2O molecules.

Central-Line Slope Analysis. For more quantitative analysis, we used the central-line slope (CLS) method[87] that recently has been extended to systems with non-Gaussian dynamics.[88−91] At each spectral cut along the ω_1 frequency, the ω_3^{max} frequency is found where the spectrum peaks. The slope of the resulted function represents the frequency-dependent correlation function at a given time t:

$$C_{11}^{S}(t, \omega) \cong S(T, \omega_1) = \frac{\partial \omega_3^{max}(T, \omega_1)}{\partial \omega_1}$$

When the CLS has the maximum value of one, the excitation and probing frequencies are fully correlated. As the slope with the increase of the waiting time T decays to zero, the correlation is completely lost. The slope lines are shown in Figures 5 and 6 as black curves. In practice, instead of calculating the derivative that is sensitive to all kinds of noise, it is useful to fit several (ω_1, ω_3^{max}) points in the spectral region of interest with a linear function, and obtain the CLS value from the fit.

Figure 7 summarizes results of the CLS analysis for H_2O- (a) and HDO:D_2O-filled (b) RMs. Although straightforward extraction of slopes in the center of transition peak is not possible for waiting times >1 ps because of interference with the thermal signals, there are regions of the 2D IR spectra where the heating signal appears to be displaced from the signal provided by the 0−1 OH vibrational transition. For instance, this occurs at the excitation frequency around 3600 cm^{-1}, thereby providing a window of opportunity to analyze transition frequency dynamics at time scales longer than vibrational relaxation (hereby lending additional support to the 2D IR spectroscopy as compared to frequency-integrated techniques such as echo-peak shift).

Both HDO:D_2O and H_2O CLS transients shown in Figure 7 look similar: after a minor drop during the first 250−500 fs, they recover and remain at high levels until as long as 5 ps delays. The peculiar non-monotonic behavior of CLS within 1 ps is related to the different relaxation rates of core and shell subensembles of water molecules. It was shown previously that relaxation of OH stretch vibrations in the shell and core of H_2O-filled RMs occurs at time scales of ∼0.3 and ∼1 ps, respectively.[32] As a result, at short (<0.1 ps for H_2O) waiting times, the overall response is a weighted average of the core (share of 0.6 in number of OH oscillators) and shell (∼0.4) responses with core dynamics being faster than the shell ones. As a result, the CLS function dives at short times. At longer waiting times, the core water response vanishes because of vibrational relaxation, and the shell water subensemble contributes most to the experimental 2D IR spectrum.[30] Similar behavior has been observed before in transient anisotropy measurements[30,46] and will be discussed in more detail later in the text.

The pronounced correlations in the OH stretch vibrational frequency observed at long waiting times support the conclusion about extremely slow dynamics of the excited OH stretch vibrations. Such behavior in turn signifies a number of phenomena specific for interfacial water. This includes "frozen" structural dynamics in the RM environment, low intermolecular couplings between water molecules, and probably even suppression of intramolecular exchange between vibrational modes.

The correlation function for interfacial isotopically undiluted water (i.e., with intra- and potentially intermolecular interactions allowed) has never been reported before. However, similar results have been previously obtained for HDO dissolved in the water in w = 2 RMs.[23,52,92] The correlation function decay, estimated from the spectrally integrated photon echo-peak shift, indicates the two different time scales of 0.25 to 15 ps,[92] with no dip and recovery reported here. Most

dx.doi.org/10.1021/jp405853j | J. Phys. Chem. B XXXX, XXX, XXX−XXX

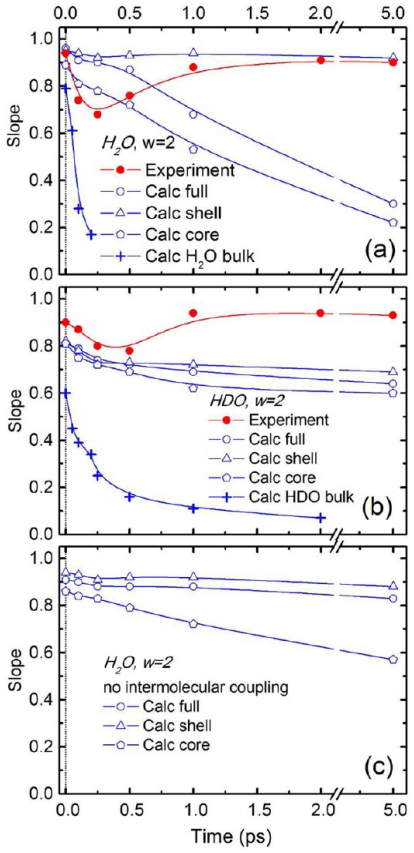

Figure 7. Results of the slope analysis of the 2D IR spectra for H_2O (a) and HDO-filled (b) RMs (w = 2). In part c, the intermolecular coupling between OH stretches was set to zero in calculations. Red circles and open blue symbols show the analysis of the experimental data and calculations, respectively. Open blue circles, all contributions are included; hexagons, the core waters only; triangles, the shell waters only. The experimental values result from the linear fit within the 3550−3600 cm^{-1} spectral region, while for the calculated data the region was extended to 3400−3600 cm^{-1} to enhance the fit stability. For comparison, the slopes for bulk H_2O and HDO simulations are also shown by blue crosses. Solid curves are guides for the eye.

probably, the integrated echo-peak shift technique used mixed vibrational responses from the core and shell water. In the case of experiments on OD oscillators of the HDO molecule, a spectral overlap with surfactant absorption may also play a role.[23] The 2D correlation technique uniquely allows us to separate responses of different water subensembles in the spectrum, as well as distinguish changes in vibrational frequency due to environment changes from the macroscopic heating to determine more accurately the aqueous environment dynamics.

Calculated 2D IR Spectra. To get a more detailed understanding of RM structure and dynamics from the experimental data, we performed theoretical calculation of 2D IR spectra shown as second-row panels in Figures 5 and 6. The calculated 2D IR spectra capture most essential features of experimental ones, including 0−1 transition bleaching signal and 1−2 transition photoinduced absorption. At short times <0.5 ps, when the population relaxation and the heating effects do not have much influence on the spectroscopic observables, our modeling directly reproduces complete 2D IR spectra, including strong initial inhomogeneity. We note that the experimental 2D IR spectra are slightly narrower and blue-shifted because a spectral filtering effect[93] is caused by the limited bandwidth of the excitation pulses.

At longer waiting times >0.5 ps, the population decay starts affecting experimental data, and the calculated spectra in the central region deviate from the observed ones. The model used involves no coupling of stretching modes to other degrees of freedom (like the bending mode and its overtone)[14] and hence does not account for vibrational relaxation.[14,34] In other words, the calculations treat dynamics of the core and shell subensembles at the same footing. Overestimation of the core water contribution to the modeled spectra can also be seen in poor reproduction of CLS dynamics (open circles in Figure 7a,b): while the experimental value returns to constantly high values at long times, the calculated CLS persistently decays regardless of the time. At the same time, the temperature increase resulting from the vibrational relaxation of OH stretches to lower frequency (thermal) modes introduces another feature in the experimental 2D IR spectra (at approximately ω_1 = 3500 cm^{-1}, ω_3 = 3450 cm^{-1}). This leads to an additional visual discrepancy between experimental and calculated spectra, which should not be forgotten while comparing the two.

To account for this complication, we disentangled the contributions from different subensembles of water and calculated 2D IR spectra representing the core and shell water contributions separately. Two bottom rows in Figures 5 and 6 clearly indicate that experimental results at long waiting times fit best the calculations for the shell subensemble. Both the spectrum shape and CLS dynamics for H_2O-filled RMs (Figure 7a, triangles) are also very well reproduced by the calculation for the shell water, confirming that the core subensemble does not contribute substantially to experimental observables after 1 ps.

The CLS for the core water (Figure 7a, pentagons) decays much faster than for the shell. Switching off the intermolecular interactions (Figure 7c) provides some insight into such behavior: the shell dynamics do not change, while the core dynamics decelerate. Therefore, first, intermolecular interactions play no role for shell water, and, second, they accelerate the core dynamics through sharing OH excitation among several OH oscillators—the mechanism known for bulk water.[15] However, core water dynamics are still much slower than in the bulk (Figure 7a, crosses) which signifies the nanoconfinement effect due to inevitable localization of the stretch excitation because of a finite amount of water molecules in the core.

In the simulated shell water spectra for the H_2O-filled RMs, two distinct diagonal peaks are observed at $\omega_{1,3} \sim$ 3500 and ~3600 cm^{-1}, along with the corresponding cross-peak developing at longer times (Figure 5). In the experimental data, such features can also be discerned at 0.25 and 0.5 ps waiting times when the core water contribution has already decayed but the thermal response has not yet taken over. For the isotopically diluted water, this double peak structure is completely absent (Figure 6). This points to its intramolecular origin, where the intramolecular coupling splits the vibrations in two peaks with symmetric and asymmetric mode character, much like is observed for isolated water molecules in weak hydrogen bonding environment.[94] If the two-peak structure had been dominated by a splitting into strongly and weakly hydrogen-bound OH stretches, it would have been preserved for isotopically diluted water, which is not the case. Still, as discussed in ref 21, the modes are not purely symmetric nor

dx.doi.org/10.1021/jp405853j | J. Phys. Chem. B XXXX, XXX, XXX−XXX

asymmetric, as on average the modes are delocalized on ~1.5 OH stretches. The cross-peaks between the two modes are even more pronounced in 2D spectra measured for the cross-polarized pump and probe beams (not shown), as expected for the case of orthogonal modes. However, a more detailed discussion on the symmetric and asymmetric modes of the shell water and their population exchange goes beyond the scope of this paper.

In the simulated slopes for HDO:D_2O-filled RMs (Figure 7b), little difference was found between the dynamics of the two subensembles. As the shell waters are embedded into the membrane while the core water are more in the bulk-like phase, their similar spectral dynamics may seem odd. However, it is important to realize that the core water is defined in such a way that it includes water molecules that donate one hydrogen bond to the surfactant. These waters are immobilized as compared to bulk water, causing the fully hydrogen-bound water in the center of the micelle to be partially immobilized, too. The core water in small RMs is thus not much more mobile than the shell water, as reflected in the slopes, and both are much slower than the bulk water.

At the waiting times of 0 and 0.1 ps antidiagonal cross sections of the 0−1 transition in the modeled 2D IR spectra for HDO:D_2O RMs are slightly wider than in the experimental spectra. As the antidiagonal width is indicative of homogeneous broadening, the predicted initial CLS for HDO:D_2O is noticeably lower than the experimental one (Figure 7b). This is a direct consequence of the librational component in the dynamics of water having a strong effect at sub-100 fs time scale.[85,86,95,96] The effect of librations is generally overestimated in the molecular dynamics simulations and the corresponding calculations of vibrational response.[97] Curiously enough, such an effect is not observed for H_2O-filled RMs (Figure 5). This in fact is purely coincidental and can be traced back to the more complex shape of the H_2O vibrational spectrum (Figure 2). Broadening of the absorption contour stretches the 2D peak along the diagonal, thereby effectively leading to increased inhomogeneity and higher CLS values.[98,99] The very same effect accounts for the lower initial values of the calculated CLS for HDO than for H_2O (crosses in Figure 7a and b), and for persistently higher slope values for H_2O-filled RMs as compared to the HOD-filled ones.

Summarizing the above discussion on matching the experimental and theoretical 2D IR spectra, we conclude that calculated 2D IR spectra reproduce well the early waiting time (<0.5 ps) experimental data. However, at longer times, the experiment represents mostly the response of the shell water and therefore should be compared to the calculations for this subensemble only. At 5 ps delay, only the blue shoulder of experimentally observed 2D IR peak could be used in the analysis to avoid interference with the sample-heating response.

DISCUSSION: MOLECULAR PICTURE OF MICELLE-CONFINED WATER

For the shell subensemble, the exceptionally long correlation memory observed in the 2D experiment and confirmed by the calculations uncovers some special properties of interfacial water. On one hand, frequencies of the vibrational transitions depend on the water hydrogen bonding to the surrounding, so that spectral diffusion reflects changes imposed upon the hydrogen bond strength by their dynamical settings. From this point of view, the slow spectral diffusion we observe in small RMs filled with HDO:D_2O implies diminutive structural variations in the hydrogen bonding environment. On the other hand, in systems with a high density of resonantly coupled oscillators like pure H_2O, intermolecular energy transfer induces a substantial change in the oscillator frequencies.[15,96] This however has little to do with the environmental dynamics: as the excitation hops between waters in slightly different settings, the transition frequencies of excited vibrational modes decorrelate. From this viewpoint, the negligible spectral diffusion in w = 2 RMs filled with H_2O is a sign of an inefficient intermolecular energy transfer and hence a weak coupling between the water molecules in the interfacial layer.

The efficiency of intermolecular energy transfer is dictated by the intermolecular couplings, the vibrational frequency gaps, and the fluctuation of these quantities. Furthermore, the abundance of oscillators will determine if transfer is possible at all. While the intermolecular couplings, the frequency gaps, and the fluctuations are affected by the interaction with the lipid wall, the dominant effect for the shell water is the isolation of the molecules from each other. To prove this point, we calculated histograms of the probability distribution of the inter- and intramolecular couplings in subensembles (Figure 8).

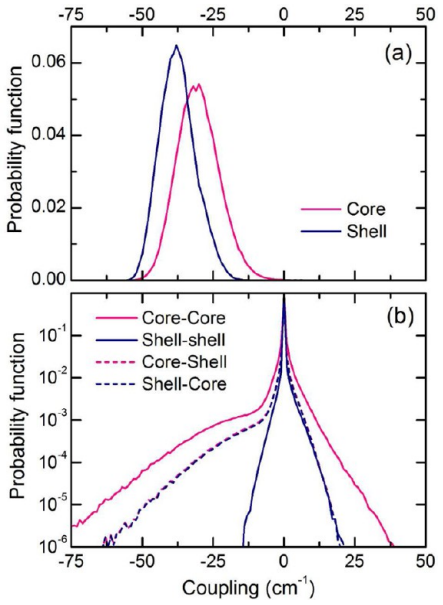

Figure 8. Histograms of the distribution of the intra- (a) and intermolecular (b) couplings for the different subensembles: core (magenta) and shell (navy). In part b, dashed curves show the histograms for the coupling between water molecules belonging to different subensembles.

The *intra*molecular coupling in the shell molecules peaks at −38 cm^{-1}, while in the core subensemble the peak value is −30 cm^{-1} (Figure 8a). The difference is because intramolecular coupling depends on hydrogen bonding which is stronger for the core molecules. For instance, in the gas phase, the coupling is the highest (−58 cm^{-1}), while, in the bulk, it amounts to only −27 cm^{-1}.[78] The *inter*molecular couplings (Figure 8b) between core water molecules are larger than those between core and shell as well as between shell molecules, which typically have couplings weaker than 10 cm^{-1}. This results in limited communication between the waters in the hydration shell of RM. The sharp peak around zero reflects a simple fact that the

dx.doi.org/10.1021/jp405853j | J. Phys. Chem. B XXXX, XXX, XXX−XXX

coupling between two OH oscillators becomes negligibly small if the oscillators are far apart, as most of the pairs are.

The extent of the coupling reduction between water molecules in RMs can be estimated through the vibrational population dynamics, which were investigated by calculating the probability that, if a particular OH stretch was initially excited, it will retain the excitation at later times. These population transfer probabilities are shown in Figure 9a, both

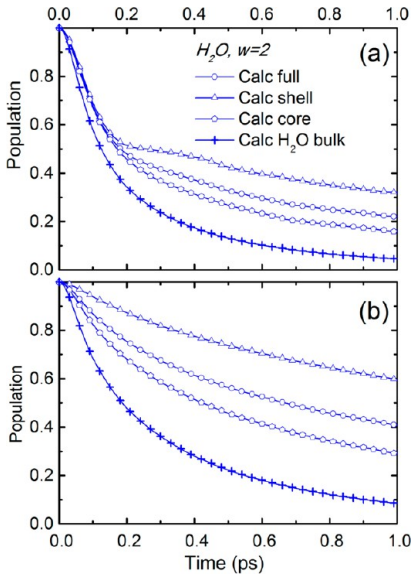

Figure 9. Vibrational population survival of the initially excited OH stretch (a) and a water molecule (b). Open blue circles, all contributions are included; hexagons, the core waters only; triangles, the shell waters only; crosses, bulk water (for reference).

for the full ensemble and for the two subensembles. Results for bulk water obtained in ref 43 are also included for comparison. For short times (<200 fs), the population of an excited OH stretch is lost at approximately the same rate for both subensembles but slightly slower than for bulk water due to the reduced coupling between molecules. At longer times, the core water OH oscillators lose population much faster than the shell water. This difference can be understood by looking at how long the excitation keeps on sitting at the same molecule. For this, the probability that a particular OH stretch was initially excited and the excitation is still localized on the same molecule at a later time was also calculated (Figure 9b). For shell water, very few excitations leave the initially excited molecule, so that we can conclude that for shell molecules the intramolecular population redistribution dominates. For core water, both the inter- and intramolecular processes are approximately equally important, which is in sharp contrast with bulk water where the intermolecular population transfer dominates.[43] This is again a signature of the nanoconfinement effect resulting from the reduced ability of the OH stretch vibration to delocalize outside the core due to its truncation.

Finally, the polarization anisotropy was calculated using the response functions for $\tau_1 = 0$ and $\tau_3 = 0$ as described in ref 100. The anisotropy was obtained from the signals with parallel ($S_{\|}$) and perpendicular (S_p) configurations of the pump and probe pulses $r(t) = (S_{\|} - S_p)/(S_{\|} + 2S_p)$. This was performed separately for the full system (i.e., H_2O-filled RMs), nullifying all the couplings (mimicking the HOD-in-D_2O-filled RMs) and neglecting intermolecular couplings only (Figure 10). While in all cases the anisotropy decay in RMs is slower than in bulk water, the details of slowing down depend on the particular case.

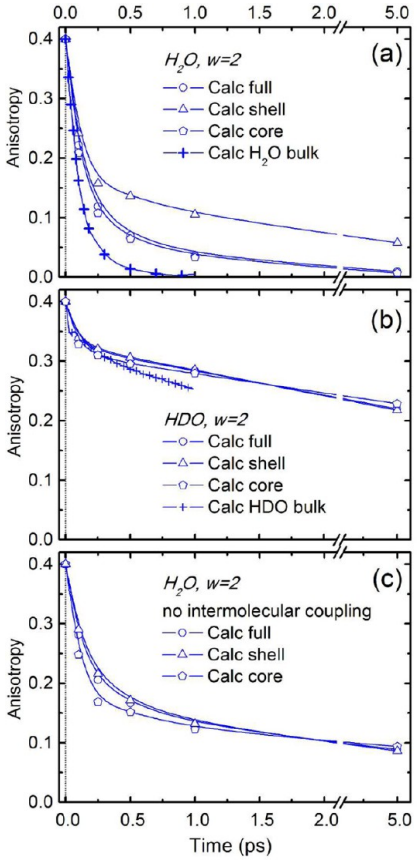

Figure 10. Transient anisotropies calculated for H_2O- (a) and HDO:D_2O-filled (b) RMs (w = 2). In part c, the intermolecular coupling between OH stretches was set to zero in calculations. Open blue circles, all contributions are included; hexagons, the core waters only; triangles, the shell waters only. For comparison, the slopes for bulk H_2O and HDO:D_2O simulations are also shown by blue crosses. Solid curves are guides for the eye.

For H_2O-filled RMs, the shell water anisotropy is the slowest (Figure 10a). Nullifying the intermolecular couplings does not have a noticeable change on the anisotropy decay (Figure 10c). From this, we conclude that the anisotropy decay of the shell water simply reflects the intramolecular population transfer between the symmetric and asymmetric modes that have orthogonal transient dipole moments.[46] In contrast, the core water anisotropy slows down when the intermolecular interactions are switched off. This means that both intra- and intermolecular couplings are important for explaining core water anisotropy dynamics. Note that these dynamics are still considerably slower than those for bulk water (Figure 10a, crosses) where the intermolecular interactions completely dominate. Therefore, for the shell water, the overall intermolecular couplings are reduced because of the finite number of partners, as only 30 water molecules form the core. This sets a limit in the number of neighboring water molecules over which the excitation can be redistributed, which is in essence the nanoconfinement effect.

The calculated anisotropy of HOD:D_2O-filled micelles (Figure 10b) reproduces well the experimental results.[30,52]

dx.doi.org/10.1021/jp405853j | J. Phys. Chem. B XXXX, XXX, XXX−XXX

Interestingly, little difference is found between the anisotropies for the core and shell water subensembles. Similar to the slopes (Figure 7b), this is a result of including the water molecules donating one hydrogen bond to a surfactant molecule into the core subensemble. These water molecules have few alternative hydrogen bond partners due to the presence of counterions in this region and thus have limited possibilities for rotation.

The fact that energy transfer and couplings between the molecules in small RMs are suppressed is consistent with previous MD simulations which indicated considerable variations in the water structure and density as well as a presence of ionic "isolation" layers in the vicinity of lipid interface.[38,39] We anticipate mostly the suppressed dynamics of the environment to be responsible for decreasing the vibrational excitation mobility. This interpretation is confirmed by the slow CLS dynamics (Figure 7a) as well as anisotropy and population transfer deduced in the current study (Figures 9 and 10), which are qualitatively consistent with the correlation functions presented in previous MD simulations.[12,38]

The picture of the interfacial water layer which comes to our view represents an ensemble of noninteracting quasi-monomeric water molecules embedded into a relatively stable (at the experimental time scale) matrix of lipid heads, tails, and positive counterions. This picture is clearly different from a flexible dynamical network of strongly linked water molecules considered to have a place in bulk water. The limited communication between the shell water molecules and other water molecules observed in experimental data stems from the reduced coupling between them. On top of this comes the reduced frequency fluctuations imposed by environment, and the frequency mismatch between shell and core water molecules (Figure 2). This is in line with previous observations made for the (1,2-dimyristoyl-*sn*-glycero-3-[phospho-L-serine]) lipid water interface that membrane-bound water communicates little with bulk-like water in the vicinity.[101]

CONCLUSIONS

In this paper, we used 2D IR spectroscopy of water OH stretch vibrations, molecular dynamics simulations, and theoretical calculations of vibratonal spectra to elucidate the vibrational and structural dynamics of water confined in small reverse micelles. We found that the water molecules can be divided into two subensembles consisting of water-bound water molecules in the core and surfactant-bound water molecules at the interface. We observed that these subensembles communicate very little with each other and demonstrate different organization and dynamics. The environment fluctuations are slowed down for the shell water molecules. These are attached to the lipid interface and decoupled from one another and from the surrounding core water. On the other hand, the water-bound water in the core demonstrates more bulk-like behavior. However, as shown by the theoretical calculations, the energy transfer in the core is slowed down considerably due to nanoconfinement of the vibrational excitations.

Our model predicts that both the vibrational and orientational dynamics of water molecules in the core of the RMs are considerably slower than in bulk water. For the HOD:D_2O-filled RMs, the spectral diffusion is similar for core and shell water but considerably slower than for bulk water. This reflects the fact that the hydrogen bond network in the RMs core is much more stable: on one hand, many molecules in the core are still singly hydrogen-bonded to the static membrane, and on the other hand, other water molecules have fewer partners for hydrogen bond exchange.[102,103] Because of that, it does not seem possible to make any conclusions on nanoconfinment of the core water on the basis of experimental data (despite the claims in ref 31), as the shell and core waters provide no contrast parameter to differentiate between them. In contrast, for H_2O-filled RMs, the spectral diffusion is strongly accelerated for the core water as compared to the shell water (albeit still being much slower than in bulk) due to the possibility for the excitations to move around between different water molecules, which is impossible in the shell. This difference in the excitation transfer can be attributed to the density and dynamics of surrounding vibrational oscillators, and is also reflected in the observable difference in CLSs (Figure 7a) and the anisotropy (Figure 10a). The former provides the unequivocal experimental evidence of the nanoconfinement effect[30,31,104] on water dynamics in small RMs.

The observed discrepancies between theory and experiment, such as, for instance, the overestimation of the simulated shell water dynamics (reflected in the lower CLS values at long times for theory as compared to the experiment), may arise from a number of reasons. First, the force field used may not correctly account for the abundance of the different kinds of shell water.[40] Second, the employed force fields have never been optimized to describe dynamics of the complex RM system at hand. The ongoing force field developments may allow improving agreement in the future.[105] Finally, population relaxation of the OH stretch, which is not described in the framework of the current spectral simulations, is significant in the experimental data where it gives rise to the decay of the core water response and subsequent rise of the thermal signal. Developments in theory may allow in the future the inclusion of such effects.[106] Nevertheless, the qualitative agreement with experiment is convincing enough, while the differences observed between the shell, core, and bulk water simulations are robust, providing clear evidence for the nanoconfinement effect of the core water in RMs.

The findings presented in this paper provide a picture of water in the vicinity of biomolecules like membranes or proteins, where a number of water molecules are essentially embedded as "crystal" water in the biomolecule or the first few water layers are immobilized and restricted in their ability to redistribute energy near the surface. The water molecules embedded in the lipid membrane are easier to observe than the surface water molecules in conventional measurements like X-ray diffraction and NMR. However, we found that the surface water is also strongly influenced by the presence of the biomolecules.

AUTHOR INFORMATION

Notes

The authors declare no competing financial interest.
[§]P.A.P. is deceased.

ACKNOWLEDGMENTS

J.L.S. acknowledges support from grant DOE DE-FG02-09ER16110.

REFERENCES

(1) Singer, S. J.; Nicolson, G. L. The Fluid Mosaic Model of the Structure of Cell Membranes. *Science* **1972**, *175*, 720−731.
(2) Ball, P. Water as an Active Constituent in Cell Biology. *Chem. Rev.* **2008**, *108*, 74−108.

(3) Engelman, D. M. Membranes are More Mosaic than Fluid. *Nature* **2005**, *438*, 578−580.
(4) Milhaud, J. New Insights into Water-Phospholipid Model Membrane Interactions. *Biochim. Biophys. Acta, Biomembr.* **2004**, *1663*, 19−51.
(5) Krepkiy, D.; Mihailescu, M.; Freites, J. A.; Schow, E. V.; Worcester, D. L.; Gawrisch, K.; Tobias, D. J.; White, S. H.; Swartz, K. J. Structure and Hydration of Membranes Embedded with Voltage-Sensing Domains. *Nature* **2009**, *462*, 473−479.
(6) Kurze, V.; Steinbauer, B.; Huber, T.; Beyer, K. A 2H NMR Study of Macroscopically Aligned Bilayer Membranes Containing Interfacial Hydroxyl Residues. *Biophys. J.* **2000**, *78*, 2441−2451.
(7) Zhou, Z.; Sayer, B. G.; Hughes, D. W.; Stark, R. E.; Epand, R. M. Studies of Phospholipid Hydration by High-Resolution Magic-Angle Spinning Nuclear Magnetic Resonance. *Biophys. J.* **1999**, *76*, 387−399.
(8) Klösgen, B.; Reichle, C.; Kohlsmann, S.; Kramer, K. D. Dielectric Spectroscopy as a Sensor of Membrane Headgroup Mobility and Hydration. *Biophys. J.* **1996**, *71*, 3251−3260.
(9) Baruah, B.; Roden, J. M.; Sedgwick, M.; Correa, N. M.; Crans, D. C.; Levinger, N. E. When Is Water Not Water? Exploring Water Confined in Large Reverse Micelles Using a Highly Charged Inorganic Molecular Probe. *J. Am. Chem. Soc.* **2006**, *128*, 12758−12765.
(10) Pileni, M. P. Reverse Micelles as Microreactors. *J. Phys. Chem.* **1993**, *97*, 6961−6973.
(11) Melo, E. P.; Aires-Barros, M. R.; Cabral, J. M. S. In *Biotechnology Annual Review*; Elsevier: 2001; Vol. 7, pp 87−129.
(12) Faeder, J.; Ladanyi, B. M. Molecular Dynamics Simulations of the Interior of Aqueous Reverse Micelles. *J. Phys. Chem. B* **2000**, *104*, 1033−1046.
(13) Abel, S.; Sterpone, F.; Bandyopadhyay, S.; Marchi, M. Molecular Modeling and Simulations of AOT−Water Reverse Micelles in Isooctane: Structural and Dynamic Properties. *J. Phys. Chem. B* **2004**, *108*, 19458−19466.
(14) Lindner, J.; Vohringer, P.; Pshenichnikov, M. S.; Cringus, D.; Wiersma, D. A.; Mostovoy, M. Vibrational Relaxation of Pure Liquid Water. *Chem. Phys. Lett.* **2006**, *421*, 329−333.
(15) Kraemer, D.; Cowan, M. L.; Paarmann, A.; Huse, N.; Nibbering, E. T. J.; Elsaesser, T.; Miller, R. J. D. Temperature Dependence of the Two-Dimensional Infrared Spectrum of Liquid H_2O. *Proc. Natl. Acad. Sci. U.S.A.* **2008**, *105*, 437−442.
(16) Tokmakoff, A. Shining Light on the Rapidly Evolving Structure of Water. *Science* **2007**, *317*, 54−55.
(17) Piletic, I. R.; Tan, H. S.; Fayer, M. D. Dynamics of Nanoscopic Water: Vibrational Echo and Infrared Pump-Probe Studies of Reverse Micelles. *J. Phys. Chem. B* **2005**, *109*, 21273−21284.
(18) Gilijamse, J. J.; Lock, A. J.; Bakker, H. J. Dynamics of Confined Water Molecules. *Proc. Natl. Acad. Sci. U.S.A.* **2005**, *102*, 3202−3207.
(19) Costard, R.; Elsaesser, T. Femtosecond OH Bending Dynamics of Water Nanopools Confined In Reverse Micelles. *J. Phys. Chem. B* **2013**, DOI: 10.1021/jp403559d.
(20) Kumar, S. K. K.; Tamimi, A.; Fayer, M. D. Dynamics in the Interior of AOT Lamellae Investigated with Two-Dimensional Infrared Spectroscopy. *J. Am. Chem. Soc.* **2013**, *135*, 5118−5126.
(21) Jansen, T. l. C.; Cringus, D.; Pshenichnikov, M. S. Dissimilar Dynamics of Coupled Water Vibrations. *J. Phys. Chem. A* **2009**, *113*, 6260−6265.
(22) Levinger, N. E.; Swafford, L. A. Ultrafast Dynamics in Reverse Micelles. *Annu. Rev. Phys. Chem.* **2009**, *60*, 385−406.
(23) Fenn, E. E.; Wong, D. B.; Fayer, M. D. Water Dynamics in Small Reverse Micelles in Two Solvents: Two-Dimensional Infrared Vibrational Echoes with Two-Dimensional Background Subtraction. *J. Chem. Phys.* **2011**, *134*, 054512-1−054512-11.
(24) Moilanen, D. E.; Fenn, E. E.; Wong, D.; Fayer, M. D. Water Dynamics in Large and Small Reverse Micelles: from Two Ensembles to Collective Behavior. *J. Chem. Phys.* **2009**, *131*, 014704-01−014704-05.
(25) Moilanen, D. E.; Fenn, E. E.; Wong, D.; Fayer, M. D. Water Dynamics at the Interface in AOT Reverse Micelles. *J. Phys. Chem. B* **2009**, *113*, 8560−8568.
(26) Park, S.; Moilanen, D. E.; Fayer, M. D. Water Dynamics - The Effects of Ions and Nanoconfinement. *J. Phys. Chem. B* **2008**, *112*, 5279−5290.
(27) Zhao, W.; Moilanen, D. E.; Fenn, E. E.; Fayer, M. D. Water at the Surfaces of Aligned Phospholipid Multibilayer Model Membranes Probed with Ultrafast Vibrational Spectroscopy. *J. Am. Chem. Soc.* **2008**, *130*, 13927−13937.
(28) Tan, H. S.; Piletic, I. R.; Fayer, M. D. Orientational Dynamics of Water Confined on a Nanometer Length Scale in Reverse Micelles. *J. Chem. Phys.* **2005**, *122*, 174501−174509.
(29) Dokter, A. M.; Petersen, C.; Woutersen, S.; Bakker, H. J. Vibrational Dynamics of Ice in Reverse Micelles. *J. Chem. Phys.* **2008**, *128*, 044509-01−044509-07.
(30) Dokter, A. M.; Woutersen, S.; Bakker, H. J. Inhomogeneous Dynamics in Confined Water Nanodroplets. *Proc. Natl. Acad. Sci. U.S.A.* **2006**, *103*, 15355−15358.
(31) Dokter, A. M.; Woutersen, S.; Bakker, H. J. Anomalous Slowing Down of the Vibrational Relaxation of Liquid Water upon Nanoscale Confinement. *Phys. Rev. Lett.* **2005**, *94*, 178301-1−178301-4.
(32) Cringus, D.; Bakulin, A.; Lindner, J.; Pshenichnikov, M. S.; Vohringer, P.; Wiersma, D. A. Ultrafast Energy Transfer in Water-AOT Reverse Micelles. *J. Phys. Chem. B* **2007**, *111*, 14193−14207.
(33) Cringus, D.; Lindner, J.; Milder, M. T. W.; Pshenichnikov, M. S.; Vohringer, P.; Wiersma, D. A. Femtosecond Water Dynamics in Reverse-Micellar Nanodroplets. *Chem. Phys. Lett.* **2005**, *408*, 162−168.
(34) Costard, R.; Levinger, N. E.; Nibbering, E. T. J.; Elsaesser, T. Ultrafast Vibrational Dynamics of Water Confined in Phospholipid Reverse Micelles. *J. Phys. Chem. B* **2012**, *116*, 5752−5759.
(35) Levinger, N. E.; Costard, R.; Nibbering, E. T. J.; Elsaesser, T. Ultrafast Energy Migration Pathways in Self-Assembled Phospholipids Interacting with Confined Water. *J. Phys. Chem. A* **2011**, *115*, 11952−11959.
(36) Correa, N. M.; Silber, J. J.; Riter, R. E.; Levinger, N. E. Nonaqueous Polar Solvents in Reverse Micelle Systems. *Chem. Rev.* **2012**, *112*, 4569−4602.
(37) Riter, R. E.; Undiks, E. P.; Levinger, N. E. Impact of Counterion on Water Motion in Aerosol OT Reverse Micelles. *J. Am. Chem. Soc.* **1998**, *120*, 6062−6067.
(38) Chowdhary, J.; Ladanyi, B. M. Molecular Dynamics Simulation of Aerosol-OT Reverse Micelles. *J. Phys. Chem. B* **2009**, *113*, 15029−15039.
(39) Faeder, J.; Ladanyi, B. M. Solvation Dynamics in Aqueous Reverse Micelles: A Computer Simulation Study. *J. Phys. Chem. B* **2001**, *105*, 11148−11158.
(40) Martinez, A. V.; Dominguez, L.; Małolepsza, E.; Moser, A.; Ziegler, Z.; Straub, J. E. Probing the Structure and Dynamics of Confined Water in AOT Reverse Micelles. *J. Phys. Chem. B* **2013**, *117*, 7345−7351.
(41) Stahla, M. L.; Baruah, B.; James, D. M.; Johnson, M. D.; Levinger, N. E.; Crans, D. C. 1H NMR Studies of Aerosol-OT Reverse Micelles with Alkali and Magnesium Counterions: Preparation and Analysis of MAOTs. *Langmuir* **2008**, *24*, 6027−6035.
(42) Harpham, M. R.; Ladanyi, B. M.; Levinger, N. E.; Herwig, K. W. Water Motion in Reverse Micelles Studied by Quasielastic Neutron Scattering and Molecular Dynamics Simulations. *J. Chem. Phys.* **2004**, *121*, 7855−7868.
(43) Jansen, T. L. C.; Auer, B. M.; Yang, M.; Skinner, J. L. Two-Dimensional Infrared Spectroscopy and Ultrafast Anisotropy Decay of Water. *J. Chem. Phys.* **2010**, *132*, 7.
(44) Maitra, A. Determination of Size Parameters of Water-Aerosol OT-Oil Reverse Micelles from their Nuclear Magnetic Resonance Data. *J. Phys. Chem.* **1984**, *88*, 5122−5125.
(45) Piletic, I. R.; Moilanen, D. E.; Spry, D. B.; Levinger, N. E.; Fayer, M. D. Testing the Core/Shell Model of Nanoconfined Water in Reverse Micelles Using Linear and Nonlinear IR Spectroscopy. *J. Phys. Chem. A* **2006**, *110*, 4985−4999.
(46) Bakulin, A. A.; Pshenichnikov, M. S. Reduced Coupling of Water Molecules near the Surface of Reverse Micelles. *Phys. Chem. Chem. Phys.* **2011**, *13*, 19355−19361.

(47) Skinner, J. L.; Auer, B. M.; Lin, Y. S. *Advances in Chemical Physics*; John Wiley & Sons Inc: New York, 2009; Vol. *142*, pp 59−103.
(48) Asbury, J. B.; Steinel, T.; Stromberg, C.; Corcelli, S. A.; Lawrence, C. P.; Skinner, J. L.; Fayer, M. D. Water Dynamics: Vibrational Echo Correlation Spectroscopy and Comparison to Molecular Dynamics Simulations. *J. Phys. Chem. A* **2004**, *108*, 1107−1119.
(49) Loparo, J. J.; Roberts, S. T.; Tokmakoff, A. Multidimensional Infrared Spectroscopy of Water. II. Hydrogen Dond Switching Dynamics. *J. Chem. Phys.* **2006**, *125*, 194522-01−194522-12.
(50) Garrett-Roe, S.; Perakis, F.; Rao, F.; Hamm, P. Three-Dimensional Infrared Spectroscopy of Isotope-Substituted Liquid Water Reveals Heterogeneous Dynamics. *J. Phys. Chem. B* **2011**, *115*, 6976−6984.
(51) Bakulin, A. A.; Cringus, D.; Pshenichnikov, M. S.; Wiersma, D. A. Frozen Dynamics and Insulation of Water at the Lipid Interface. *Ultrafast Phenomena XVI* **2009**, 514−516.
(52) Fenn, E. E.; Wong, D. B.; Giammanco, C. H.; Fayer, M. D. Dynamics of Water at the Interface in Reverse Micelles: Measurements of Spectral Diffusion with Two-Dimensional Infrared Vibrational Echoes. *J. Phys. Chem. B* **2011**, *115*, 11658−11670.
(53) Rosenfeld, D. E.; Nishida, J.; Yan, C.; Kumar, S. K. K.; Tamimi, A.; Fayer, M. D. Structural Dynamics at Monolayer−Liquid Interfaces Probed by 2D IR Spectroscopy. *J. Phys. Chem. C* **2012**, *117*, 1409−1420.
(54) Woutersen, S.; Bakker, H. J. Resonant Intermolecular Transfer of Vibrational Energy in Liquid Water. *Nature* **1999**, *402*, 507−509.
(55) Graener, H.; Seifert, G.; Laubereau, A. Vibrational and Reorientational Dynamics of Water Molecules in Liquid Matrices. *Chem. Phys.* **1993**, *175*, 193−204.
(56) Pieniazek, P. A.; Lin, Y.-S.; Chowdhary, J.; Ladanyi, B. M.; Skinner, J. L. Vibrational Spectroscopy and Dynamics of Water Confined inside Reverse Micelles. *J. Phys. Chem. B* **2009**, *113*, 15017−15028.
(57) Faeder, J.; Albert, M. V.; Ladanyi, B. M. Molecular Dynamics Simulations of the Interior of Aqueous Reverse Micelles: A Comparison Between Sodium and Potassium Counterions. *Langmuir* **2003**, *19*, 2514−2520.
(58) Pomata, M. H. H.; Laria, D.; Skaf, M. S.; Elola, M. D. Molecular Dynamics Simulations of AOT-Water/Formamide Reverse Micelles: Structural and Dynamical Properties. *J. Chem. Phys.* **2008**, *129*, 244503−244509.
(59) Senapati, S.; Berkowitz, M. L. Water Structure and Dynamics in Phosphate Fluorosurfactant Based Reverse Micelle: A Computer Simulation Study. *J. Chem. Phys.* **2003**, *118*, 1937−1944.
(60) Gardner, A.; Vasquez, V.; Clifton, A.; Graeve, O. Molecular Dynamics Analysis of the AOT/Water/Isooctane System: Effect of Simulation Time, Initial Configuration, and Model Salts. *Fluid Phase Equilib.* **2007**, *262*, 264−270.
(61) Schmidt, J. R.; Corcelli, S. A.; Skinner, J. L. Pronounced non-Condon Effects in the Ultrafast Infrared Spectroscopy of Water. *J. Chem. Phys.* **2005**, *123*, 044513−044513.
(62) Hamm, P.; Lim, M. H.; Hochstrasser, R. M. Structure of the Amide I Band of Peptides Measured by Femtosecond Nonlinear-Infrared Spectroscopy. *J. Phys. Chem. B* **1998**, *102*, 6123−6138.
(63) Yeremenko, S.; Baltuska, A.; de Haan, F.; Pshenichnikov, M. S.; Wiersma, D. A. Frequency-Resolved Pump Probe Characterization of Femtosecond Infrared Pulses. *Opt. Lett.* **2002**, *27*, 1171−1173.
(64) Tauber, M. J.; Mathies, R. A.; Chen, X. Y.; Bradforth, S. E. Flowing Liquid Sample Jet for Resonance Raman and Ultrafast Optical Spectroscopy. *Rev. Sci. Instrum.* **2003**, *74*, 4958−4960.
(65) Khalil, M.; Demirdoven, N.; Tokmakoff, A. Obtaining Absorptive Line Shapes in Two-Dimensional Infrared Vibrational Correlation Spectra. *Phys. Rev. Lett.* **2003**, *90*, 047401-1−04740-4.
(66) de Boeij, W. P.; Pshenichnikov, M. S.; Wiersma, D. A. System-Bath Correlation Function Probed by Conventional and Time-Gated Stimulated Photon Echo. *J. Phys. Chem.* **1996**, *100*, 11806−11823.
(67) Berendsen, H. J. C.; Grigera, J. R.; Straatsma, T. P. The Missing Term in Effective Pair Potentials. *J. Phys. Chem.* **1987**, *91*, 6269−6271.
(68) Schweighofer, K. J.; Essmann, U.; Berkowitz, M. Simulation of Sodium Dodecyl Sulfate at the Water−Vapor and Water−Carbon Tetrachloride Interfaces at Low Surface Coverage. *J. Phys. Chem. B* **1997**, *101*, 3793−3799.
(69) Martin, M. G.; Siepmann, J. I. Novel Configurational-Bias Monte Carlo Method for Branched Molecules. Transferable Potentials for Phase Equilibria. 2. United-Atom Description of Branched Alkanes. *J. Phys. Chem. B* **1999**, *103*, 4508−4517.
(70) Weitz, S. L.; Potoff, J. J. Effect of Quadrupole Moment on the Phase Behavior of Binary Mixtures Containing Ethene. *Fluid Phase Equilib.* **2005**, *234*, 144−150.
(71) Schlenkrich, M.; Brickmann, J.; MacKerell, A. D., Jr.; Karplus, M. *Biological Membranes*; Springer: 1996; pp 31−81.
(72) Berendsen, H. J. C.; Postma, J. P. M.; Vangunsteren, W. F.; Dinola, A.; Haak, J. R. Molecular-Dynamics with Coupling to an External Bath. *J. Chem. Phys.* **1984**, *81*, 3684−3690.
(73) Auer, B. M.; Skinner, J. L. Vibrational Sum-Frequency Spectroscopy of the Liquid/Vpor Interface for Dilute HOD in D2O. *J. Chem. Phys.* **2008**, *129*, 214705−214714.
(74) Auer, B.; Kumar, R.; Schmidt, J. R.; Skinner, J. L. Hydrogen Bonding and Raman, IR, and 2D-IR Spectroscopy of Dilute HOD in Liquid D2O. *Proc. Natl. Acad. Sci. U.S.A.* **2007**, *104*, 14215−14220.
(75) Jansen, T. l. C.; Knoester, J. Nonadiabatic Effects in the Two-Dimensional Infrared Spectra of Peptides: Application to Alanine Dipeptide. *J. Phys. Chem. B* **2006**, *110*, 22910−22916.
(76) Jansen, T. l. C.; Knoester, J. Waiting Time Dynamics in Two-Dimensional Infrared Spectroscopy. *Acc. Chem. Res.* **2009**, *42*, 1405−1411.
(77) Hochstrasser, R. M. Two-Dimensional IR-Spectroscopy: Polarization Anisotropy Effects. *Chem. Phys.* **2001**, *266*, 273−284.
(78) Auer, B. M.; Skinner, J. L. Dynamical Effects in Line Shapes for Coupled Chromophores: Time-Averaging Approximation. *J. Chem. Phys.* **2008**, *128*, 224511-1−224511-10.
(79) Cringus, D.; Yeremenko, S.; Pshenichnikov, M. S.; Wiersma, D. A. Hydrogen Bonding and Vibrational Energy Relaxation in Water-Acetonitrile Mixtures. *J. Phys. Chem. B* **2004**, *108*, 10376−10387.
(80) Kumar, R.; Schmidt, J. R.; Skinner, J. L. Hydrogen Bonding Definitions and Dynamics in Liquid Water. *J. Chem. Phys.* **2007**, *126*, 204107−204112.
(81) Nomenclature by ref 12: trapped 0.32, bound to interface 0.49, free (i.e., bulk-like) 0.19; ours: 31 core (0.6) and 21 shell (0.4).
(82) Volkov, V. V.; Palmer, D. J.; Righini, R. Distinct Water Species Confined at the Interface of a Phospholipid Membrane. *Phys. Rev. Lett.* **2007**, *99*, 078302-1−078302-4.
(83) Deak, J. C.; Pang, Y.; Sechler, T. D.; Wang, Z.; Dlott, D. D. Vibrational Energy Transfer Across a Reverse Micelle Surfactant Layer. *Science* **2004**, *306*, 473−476.
(84) Yeremenko, S.; Pshenichnikov, M. S.; Wiersma, D. A. Interference Effects in IR Photon Echo Spectroscopy of Liquid Water. *Phys. Rev. A* **2006**, *73*, 021804-1−021804-4.
(85) Loparo, J. J.; Roberts, S. T.; Tokmakoff, A. Multidimensional Infrared Spectroscopy of Water. I. Vibrational Dynamics in Two-Dimensional IR Line Shapes. *J. Chem. Phys.* **2006**, *125*, 194521-1−194521-13.
(86) Yeremenko, S.; Pshenichnikov, M. S.; Wiersma, D. A. Hydrogen-Bond Dynamics in Water Explored by Heterodyne-Detected Photon Echo. *Chem. Phys. Lett.* **2003**, *369*, 107−113.
(87) Kwak, K.; Rosenfeld, D. E.; Fayer, M. D. Taking Apart the Two-Dimensional Infrared Vibrational Echo Spectra: More Information and Elimination of Distortions. *J. Chem. Phys.* **2008**, *128*, 204505-1−204505-10.
(88) Bakulin, A. A.; Liang, C.; la Cour Jansen, T.; Wiersma, D. A.; Bakker, H. J.; Pshenichnikov, M. S. Hydrophobic Solvation: A 2D IR Spectroscopic Inquest. *Acc. Chem. Res.* **2009**, *42*, 1229−1238.
(89) Bakulin, A. A.; Pshenichnikov, M. S.; Bakker, H. J.; Petersen, C. Hydrophobic Molecules Slow Down the Hydrogen-Bond Dynamics of Water. *J. Phys. Chem. A* **2011**, *115*, 1821−1829.

(90) Roy, S.; Pshenichnikov, M. S.; Jansen, T. L. C. Analysis of 2D CS Spectra for Systems with Non-Gaussian Dynamics. *J. Phys. Chem. B* **2011**, *115*, 5431−5440.
(91) Petersen, C.; Bakulin, A. A.; Pavelyev, V. G.; Pshenichnikov, M. S.; Bakker, H. J. Femtosecond Midinfrared Study of Aggregation Behavior in Aqueous Solutions of Amphiphilic Molecules. *J. Chem. Phys.* **2010**, *133*, 164514−164518.
(92) Tan, H. S.; Piletic, I. R.; Riter, R. E.; Levinger, N. E.; Fayer, M. D. Dynamics of Water Confined on a Nanometer Length Scale in Reverse Micelles: Ultrafast Infrared Vibrational Echo Spectroscopy. *Phys. Rev. Lett.* **2005**, *94*, 057405-057401−057405-057404.
(93) Yetzbacher, M. K.; Belabas, N.; Kitney, K. A.; Jonas, D. M. Propagation, Beam Geometry, and Detection Distortions of Peak Shapes in Two-Dimensional Fourier Transform Spectra. *J. Chem. Phys.* **2007**, *126*, 044511-044511−044511-044519.
(94) Wong, D. B.; Giammanco, C. H.; Fenn, E. E.; Fayer, M. D. Dynamics of Isolated Water Molecules in a Sea of Ions in a Room Temperature Ionic Liquid. *J. Phys. Chem. B* **2012**, *117*, 623−635.
(95) Asbury, J. B.; Steinel, T.; Stromberg, C.; Gaffney, K. J.; Piletic, I. R.; Goun, A.; Fayer, M. D. Hydrogen Bond Dynamics Probed with Ultrafast Infrared Heterodyne-Detected Multidimensional Vibrational Stimulated Echoes. *Phys. Rev. Lett.* **2003**, *91*, 237402-1−237402-1.
(96) Cowan, M. L.; Bruner, B. D.; Huse, N.; Dwyer, J. R.; Chugh, B.; Nibbering, E. T. J.; Elsaesser, T.; Miller, R. J. D. Ultrafast Memory Loss and Energy Redistribution in the Hydrogen Bond Network of Liquid H2O. *Nature* **2005**, *434*, 199−202.
(97) Schmidt, J. R.; Roberts, S. T.; Loparo, J. J.; Tokmakoff, A.; Fayer, M. D.; Skinner, J. L. Are Water Simulation Models Consistent with Steady-State and Ultrafast Vibrational Spectroscopy Experiments? *Chem. Phys.* **2007**, *341*, 143−157.
(98) Lazonder, K.; Pshenichnikov, M. S.; Wiersma, D. A. Easy Interpretation of Optical Two-Dimensional Correlation Spectra. *Opt. Lett.* **2006**, *31*, 3354−3356.
(99) Roberts, S. T.; Loparo, J. J.; Tokmakoff, A. Characterization of Spectral Diffusion from Two-Dimensional Line Shapes. *J. Chem. Phys.* **2006**, *125*, 084502-1−084502-1.
(100) Lin, Y. S.; Pieniazek, P. A.; Yang, M.; Skinner, J. L. On the Calculation of Rotational Anisotropy Decay, as Measured by Ultrafast Polarization-Resolved Vibrational Pump-Probe Experiments. *J. Chem. Phys.* **2010**, *132*, 174505−174508.
(101) Ghosh, A.; Campen, R. K.; Sovago, M.; Bonn, M. Structure and Dynamics of Interfacial Water in Model Lung Surfactants. *Faraday Discuss.* **2009**, *141*, 145−159.
(102) Ramasesha, K.; Roberts, S. T.; Nicodemus, R. A.; Mandal, A.; Tokmakoff, A. Ultrafast 2D IR Anisotropy of Water Reveals Reorientation During Hydrogen-Bond Switching. *J. Chem. Phys.* **2011**, *135*, 054509−054511.
(103) Laage, D.; Stirnemann, G.; Sterpone, F.; Hynes, J. T. Water Jump Reorientation: From Theoretical Prediction to Experimental Observation. *Acc. Chem. Res.* **2012**, *45*, 53−62.
(104) Bakker, H. J.; Woutersen, S.; Nienhuys, H.-K. Reorientational Motion and Hydrogen-Bond Stretching Dynamics in Liquid Water. *Chem. Phys.* **2000**, *258*, 233−245.
(105) Tainter, C. J.; Pieniazek, P. A.; Lin, Y. S.; Skinner, J. L. Robust Three-Body Water Simulation Model. *J. Chem. Phys.* **2011**, *134*, 184501−184510.
(106) Tempelaar, R.; van der Vegte, C. P.; Knoester, J.; Jansen, T. L. C. Surface Hopping Modeling of Two-Dimensional Spectra. *J. Chem. Phys.* **2013**, *138*, 164106−164110.
(107) Humphrey, W.; Dalke, A.; Schulten, K. VMD: Visual Molecular Dynamics. *J. Mol. Graphics* **1996**, *14*, 33−38.